Journal of Translational Regenerative Medicine
2026. Volume 1

Research Paper

Fabrication and In-vitro Characterization of Simvastatin-loaded Polycaprolactone/Hydroxyapatite 3D Printed Scaffolds for Bone Tissue Engineering

Mohammad Hosein Shahrezaee[1, 2], Alireza Parhiz[3*], Negin Khoshnood[4*], Alireza Mahboubian[5], Melika Sahranavard[4]

1. School of Dentistry, Tehran University of Medical Science, Tehran, Iran.
2. Department of Oral and Maxillofacial Surgery, Faculty of Dentistry, Tehran Dental Branch, Islamic Azad University, Tehran, Iran.
3. Department of Oral and Maxillofacial Surgery, School of Dentistry, Tehran University of Medical Science, Tehran, Iran.
4. Biomaterials Research Group, Department of Nanotechnology and Advanced Materials, Materials and Energy Research Center, Karaj, Iran.
5. School of Business, The Ingenuity Center Nottingham, University of Nottingham, Nottingham, United Kingdom.

Use your device to scan and read the article online

Citation Shahrezaee MH, Parhiz A, Khoshnood N, Mahboubian A, Sahranavard M. Fabrication and In-vitro Characterization of Simvastatin-loaded Polycaprolactone/Hydroxyapatite 3D Printed Scaffolds for Bone Tissue Engineering. Journal of Translational Regenerative Medicine. 2025; 1:E1007. http://dx.doi.org/10.32598/JTRM.1.1007

http://dx.doi.org/10.32598/JTRM.1.1007

ABSTRACT

Background: Three-dimensional (3D) printing application is a promising method for the development of cell-friendly bone substitutes with appropriate properties. In this study, we developed 3D polycaprolactone (PCL)-based scaffolds by 3D printing technology, and the osteogenic differentiation of pre-osteoblast MC3T3 cells on these scaffolds was evaluated.

Methods: Considering that PCL is naturally hydrophobic and lacks active interaction sites, oxygen plasma surface modification was carried out to provide a suitable hydrophilic surface for PCL-simvastatin interaction. Different HA concentrations (0.5, 1, and 1.5 % w/v) were added to PCL scaffolds, and the scaffolds with 1% HA showed good printability with interconnected porosity.

Results: The mechanical properties exhibited an increase of 2.67 times in comparison to PCL scaffolds. The addition of HA and oxygen plasma treatment increased the hydrophilicity and swelling ratio, and the final PCL scaffolds with 1%HA and simvastatin (PHPB) showed the highest percentage of biodegradation with 36.65±3.75 (%) biodegradation ratio after 21 days. The biological studies indicated that surface modification of the PCL scaffolds provided a suitable hydrophilic platform for attachment, osteogenic differentiation, and proliferation of MC3T3 cells.

Conclusion: It seems that PHPB scaffolds are promising for bone tissue regeneration applications.

Keywords: Polycaprolactone (PCL), Hydroxyapatite (HA), Fused deposition modeling 3D printing, Simvastatin, Bone tissue engineering

Article info:
Received: 22 Sep 2025
Accepted: 10 Nov 2025
Publish: 28 Jan 2026

*** Corresponding Authors:**
Negin Khoshnood, Assistant Professor.
Address: *Biomaterials Research Group, Department of Nanotechnology and Advanced Materials, Materials and Energy Research Center, Karaj, Iran.* ***Phone:*** *+98 (912) 9724550*
E-mail: *negin.khoshnood@gmail.com*

Alireza Parhiz, Associate Professor.
Address: *Department of Oral and Maxillofacial Surgery, School of Dentistry, Tehran University of Medical Science, Tehran, Iran.*
E-mail: *alirezaparhiz@gmail.com*

Highlights

- 3D-printed PCL/1% HA scaffolds showed the best printability, uniform interconnectivity, and a 2.6-fold increase in compressive strength compared to pure PCL.
- Oxygen plasma treatment significantly enhanced hydrophilicity and swelling, enabling effective simvastatin loading.
- The synergistic combination of HA, plasma modification, and simvastatin provides a highly effective platform for bone tissue engineering.

Plain Language Summary

Most of the large bone injuries require supportive scaffolds that assist in the growth of new bone. Herein, we fabricated a novel 3D-printed scaffold made from a biodegradable polymer, polycaprolactone (PCL), hydroxyapatite (HA), a mineral naturally found in bone, and simvastatin, a drug known for stimulating bone formation. This study aimed at designing scaffolds that would not only be biocompatible but also actively capable of supporting bone regeneration. These scaffolds were printed with a highly porous structure, allowing the cells to enter, attach, and grow. Adding 1% HA to PCL enhanced structural regularity, hydrophilicity, and mechanical strength. Further, we treated the surface with oxygen plasma to make it more hydrophilic. This surface treatment aided in increasing the amount of simvastatin that the scaffold could hold. The modified scaffolds absorbed more water, degraded faster in a body-like environment, and became significantly stronger, more than double the strength of pure PCL. Drug-release studies demonstrated that simvastatin could be released over several hours. Biological testing showed that scaffolds containing both HA and simvastatin supported cell adhesion, proliferation, and bone-forming activity compared to PCL alone. Cell culture on the enhanced scaffolds led to higher levels of key markers associated with bone, more deposition of calcium, and stronger signs of osteogenic differentiation. This study demonstrated that a 3D-printed PCL scaffold incorporated with HA, plasma treatment, and simvastatin can support bone healing and may be an effective candidate for future applications in bone tissue engineering.

Introduction

Bone disorders caused by bone infections, bone tumors, osteoporosis, and trauma are prevalent, with growing incidences due to aging, accidents, and obesity [1–3]. Conventional therapies, including autografts, allografts, and xenografts, face limitations, such as scarcity, high risk of disease transmission, and immune response [4, 5]. Tissue engineering promises to restore the normal function of cells and remodel the lost tissue or organs [6]. Tissue engineering seeks to develop tissue grafts for repairing bone defects using tissue engineering scaffolds through the utilization of cells, biocompatible natural or synthetic biomaterials, and bioactive molecules [7] biomaterials, cells and biomolecular signals to produce tissue constructs for tissue engineering. For bone regeneration, researchers are focusing on the use of polymeric and polymer/ceramic scaffolds seeded with osteoblasts or mesenchymal stem cells. However, the design of high-performance scaffolds in terms of mechanical, cell-stimulation and biological performance is still required. This is the first paper investigating the use of an extrusion additive manufacturing system to produce poly(ε-caprolactone. To promote cell seeding, vascularization, and the flow of nutrients, oxygen, and cellular waste products, the scaffolds should have a highly porous, interconnected structure [8–10]. On the other hand, the surface chemistry of scaffolds should also be optimized to provide a suitable platform for cell attachment, proliferation, and differentiation [11]. Conventional scaffold fabrication methods cannot precisely control and tune the geometry, uniformity, pore size distribution, and interconnectivity of the scaffolds [12]. Also, these conventional methods cannot fabricate patient-specific scaffolds with specifically designed shapes. Along with accurate deposition, particular shape, tightly regulated size and porosity, high repeatability, resolution, cost-effectiveness, and cell distribution controllability, 3D printing technology has a strong capability to meet the shortages as indicated above [13, 14]. This technology is leading to a global revolution in the medical field and has attracted significant attention in treating various diseases. Generally, 3D

printing is a process of rapid prototyping or an additive manufacturing approach to print bio-functional materials in a layer-by-layer fabrication using biomaterials from a computer-aided design (CAD) model [15].

PCL is a biocompatible and biodegradable synthetic polyester, which is mainly used in the fabrication of 3D bone scaffolds due to its good mechanical strength with high flexibility, high stability, low melting temperature, excellent printability, and ease of use [16]. However, the absence of bioactivity, biofunctionality, and poor hydrophilicity restrict its tissue engineering uses [17, 18]. Therefore, a good strategy to overcome these restrictions is to add alternative bioactive biomaterials to PCL [19]. To encourage PCL's bioactivity and cellular absorption, a variety of components, including different metals, oxides, polymers, biomolecules, and ceramic-based materials, can be added to PCL-based scaffolds [19]. Duymaz et al. [20] utilized PCL/gelatin with levan as a polysaccharide for the fabrication of 3D printing scaffolds. They indicated that the increasing levan content promoted human osteoblast cells' biocompatibility, proliferation, and adhesion. Juan et al. [21] applied beta-tricalcium phosphate (β-TCP) and bone-decellularized extracellular matrix (dECM) in 3D-printed PCL scaffolds. PCL/-TCP scaffolds containing bone dECM exhibited superb cell seeding efficiency and proliferation in vitro, as well as exceptional bone regeneration in vivo. In another work, PCL was blended with polyethylene glycol (PEG) as ink for the 3D printing of bone scaffolds. Increased hydrophilicity, cell proliferation, and total protein content were observed in the developed scaffolds [22].

The addition of inorganic fillers, such as hydroxyapatite (HA), to polycaprolactone (PCL) can enhance its osteogenic activity and mechanical properties. The incorporation of HA is attributed to its ability to enhance affinity for ECM proteins, promote osteogenic differentiation and mineralization, and exhibit comparable composition and morphology to the inorganic component of natural bone [23–25]. Roh et al. [26] added HA and MgO nanoparticles to PCL scaffolds. HA was used to provide osteoconductivity and improve compressive strength and biocompatibility. The results demonstrated that adding these nanoparticles enhanced mineralization and cellular interactions. On the other hand, simvastatin is widely used as a clinical statin drug to inhibit the occurrence of thrombosis. It was shown that simvastatin, as a very efficient drug, could promote osteoblast differentiation in vitro and enhance bone formation, and inhibit osteoclast resorption in vivo [27–29]. Rezaei et al. [30] used simvastatin-loaded graphene oxide embedded in PCL-polyurethane scaffolds for bone regeneration. The results revealed that the addition of simvastatin improved the bioactivity of the scaffolds with additional cell support and alkaline phosphatase activity for hard tissue regeneration. Therefore, simvastatin can synergistically enhance osteogenic activity on a PCL/HA scaffold and HA.

Oxygen plasma treatment is a promising method to create active sites on the surface of polymers and increase the hydrophilicity of a polymer surface by introducing hydrophilic functional groups on the scaffolds' surface [31]. Ghorbani et al. [32] demonstrated that the surface modification of PCL constructs with oxygen plasma enhanced the hydrophilic nature of the scaffolds and facilitated the simvastatin loading.

Here, we proposed simvastatin coating applied to PCL/HA scaffolds and 3D printed PCL/HA scaffolds. For simvastatin coating, the surface of PCL/HA scaffolds was functionalized using oxygen-plasma surface modification. Surface structure, wettability, chemical structure, and mechanical properties of the scaffolds were characterized. Additionally, cell culture, calcium deposition, gene expression, and flow cytometry analyses were used to assess the cell behavior of scaffolds.

Materials and Methods

Preparation of the PCL/HA composite ink

PCL (Shenzhen Esun Industrial Co, Ltd) was dissolved in chloroform (Merck, Darmstadt, Germany) at a concentration of 5% w/v. After the PCL pellets (P) dissolved completely, HA powders (2196, Merck) were individually added to the solution at three concentrations of 0.5 (PH 0.5), 1 (PH 1), and 1.5 %w/v (PH 1.5), and homogenized using mechanical stirring [33]. Then, the obtained suspensions were subjected to ultrasonication at room temperature for 1 h. The prepared suspensions were cast on Petri dishes, allowing the solvent to evaporate. The obtained films were ground and used for printing.

3D printing of scaffolds

The scaffolds were created using a fused deposition modeling (FDM N2-3Dbioprinter, 3DPLCorporation, Iran, Tehran) 3D printing technology. P and PH films that had been ground were fed into the stainless steel nozzle (D=0.5 mm), and the temperature was increased to 70 ˚C. The 3D printing system had a pneumatic controller (two bars) and three motion axes (x, y, and z). The following settings were made for the printing parameters: Temperature: 70 ˚C and print speed: 60 mm/min. The print-ready sub-models, measuring 10×10×3 mm, were created using AutoCAD software.

Surface modification with oxygen plasma and treatment with simvastatin

Oxygen-plasma surface treatment was performed on 3D-printed P and PH (P1H) scaffolds using a plasma generator (Diener, Germany) for 3 min under an applied oxygen power of 70 W, resulting in samples labeled PP and PHP, respectively. The PH and PHP samples were immersed in a simvastatin solution (5%w/v in ethanol) for 2 h and labeled PHS and PHPS, respectively [32].

Scaffold characterization

The morphologies of the 3D-printed scaffolds were analyzed using a scanning electron microscope (SEM) (S360-Cambridge). ImageJ software, version 1.46 (NIH, USA) was applied to measure pore size and porosity.

The chemical structure of scaffolds and the efficacy of modifications were assessed through AT-Fourier transform infrared spectroscopy (AT-FTIR) spectroscopic measurements. The measurements were conducted using a Bruker Vector 33 (Germany) in the reflection mode, within the spectral range of 400-4000 cm^{-1}.

The present study employed sessile drop contact angle measurements to examine the wettability of scaffolds both prior to and subsequent to surface modifications. The CA 500A contact angle measuring device was used for this purpose.

The swelling capacity of the samples was measured for 24 hours. For this purpose, the 3D-printed scaffolds were weighed, immersed in falcons containing 20 mL Phosphate buffered saline (PBS), and transferred to a thermo-shaker (37±0.5 ˚C). The samples were weighed again at each measuring time point (1, 3, 6, 12, and 24 hours). The swelling capacity of the samples was calculated according to Equation 1 [34].

$$1.\ Swellingratio\,(\%) = \frac{(W_1 - W_0)}{W_0} \times 100$$

W_0 was the initial weight, and W_1 was the wet weight of the specimen.

To measure the biodegradation rate of the samples, the dry scaffolds were first weighed to determine their initial weight and then soaked in PBS solution for 21 days. The PBS solution was refreshed every two days, and at the defined time points, the scaffolds were removed from the PBS solution and weighed. The biodegradation ratio was calculated using Equation 2 [35]:

$$2.\ \text{Biodegradationratio}(\%) = \frac{(W_2 - W_1)}{W_1} \times 100$$

W_1 was the initial weight and W_2 was the weight of the biodegraded specimens at each time point.

The compressive mechanical properties of the P and PHPS samples (8×8×8 mm) were evaluated at room temperature using an STM20 testing machine (Santam Co). The crosshead had a load cell of 1000 N and moved at a speed of 1 mm/min.

Drug release

PHS and PHPS samples were immersed in 3 mL PBS (pH 7.4) solution at 37 in stirring conditions. Then, the release of simvastatin was analyzed at predetermined time intervals (5 min, 10 min, 20 min, 30 min, 1 h, 1.5 h, 2 h, 3 h, 4 h, 5 h, 6 h, 7 h, 8 h, and 9 h) by ultraviolet-visible (UV) spectroscopy (Biochorm Biowave2, USA) at a wavelength of 235 nm.

Cell lines and cell culture

Pre-osteoblast MC3T3 cell lines were obtained from the Materials and Energy Research Center (MERC, Karaj, Iran) and were used for cellular investigations. The cells were cultured in DMEM-F12 medium (GIBCO Life Science, Great Island, NY) supplemented with 10% FBS (GIBCO Life Science, Great Island, NY) and 1% penicillin/streptomycin (GIBCO Life Science, Great Island, NY) for the purpose of the study. The cells were cultured at 37 ˚C (5% CO_2) until they reached 80% confluency, and then harvested.

Osteogenic potential evaluation

Alizarin red staining (ARS), O-cresolphthalein complexone (OCPC), and alkaline phosphatase (ALP) were performed to measure the osteogenesis of the MC3T3 cells on the scaffolds. Calcium deposition was assessed by ARS staining and the OCPC assay.

An OCPC assay was performed after 21 days of culture. The cells were subjected to lysis in a 0.5 M Ethylenediaminetetraacetic acid (EDTA) solution followed by decalcification with 0.6 N HCl at 4 ˚C for 24 hours. Calcium concentration was measured using the Calcium Colorimetric Assay Kit (Sigma-Aldrich, Germany) at 570 nm.

In order to perform ARS staining, the cultured cells were first fixed to the scaffolds for 30 min using 10% formalin. Then, the ARS solution (Sigma-Aldrich, Germany) was added, and the mixture was incubated for 45 min in the dark. After that, the stain (Sigma, USA) was dissolved in acetic acid for 15 minutes, and the absorbance was gauged at 405 nm.

The evaluation of ALP activity was conducted using the p-nitrophenyl phosphate liquid substrate system (pNPP, Sigma-Aldrich) after 14 and 21 days. To achieve the desired outcome, the cells were broken down using a 0.5 M EDTA solution. Afterward, they were exposed to an ALP substrate solution for a period of 30 minutes. During the experiment, the absorbance was monitored at 405 nm at 5-minute intervals. The Bradford method was used to report the normalized results.

Immunostaining assay

Immunostaining was performed on cell-cultured scaffolds fixed with paraformaldehyde at 21 days. The cells were treated with 0.1% Triton X-100 for 30 minutes, followed by inhibition with 10% bovine serum albumin (BSA) for 1 hour at room temperature. The scaffolds were subsequently incubated in phalloidin solution for 30 minutes to perform phalloidin staining. The phalloidin solution was prepared at a ratio of 1:40 in PBS and contained 10% BSA and 0.1% Triton X-100. DAPI staining was conducted to stain the nuclei. Fluorescence optical microscopy (Olympus, CKX53) was utilized to capture cellular images.

Quantitative assay of gene expression

Reverse transcription polymerase chain reaction (RT-PCR) analysis was used to determine the expression levels of osteoblastic phenotypic markers after 14 and 21 days. The cultivated cells were treated with the TRIzol reagent for this purpose. The suspension was then combined with chloroform before being centrifuged (15,000 rpm, 10 min). The supernatant was collected and RNA was precipitated by combining with isopropyl alcohol and centrifuging under the same conditions (15,000 rpm, 10 min). Then, the stages of washing with 70% ethanol, drying, and dissolving in diethyl pyrocarbonate-containing water were completed. The RNA was then extracted and cDNA was produced. Finally, PCR was performed using protein-2 (BMP-2) (forward primer: CAGGAAGTTGGTGAGCTGGTATA, reverse primer: TTGTGTTCGCCTGTAGTGCATA), ALP (forward primer: -TCT GAT GCAGGTCCCTATGGT, reverse primer: TTA TGG AGT AGCTTCTTCAC), and osteocalcin (OCN) (forward primer: AGCGTGGTAGTGTAGAGA, reverse primer: AGGGTAAGAGGTAAGAAG).

Statistical analysis

GraphPad Prism software, version 6 (Prism 8™, trial version) was used for data analysis. The data were presented as Mean±SD and analyzed using a one-way ANOVA. A statistically significant result was defined as having a $P<0.05$.

Results

Characterization of 3D-printed scaffolds

As shown in Figure 1a, the P, P0.5H, P1H, and P1.5H constructs were fabricated using the 3D printing technique to optimize the HA content ratio in the scaffolds for further studies. The scaffolds showed cube-like patterns with open and interconnected porous architectures, with a pore size of ~ 350 µm. The obtained pore size was optimal (100-400 µm) for osteoconductivity and bone regeneration [36, 37]. In the P, P0.5H, and P1H scaffolds, a defined and uniform architecture was observed; however, in the case of P1.5H, the structure was deformed due to the aggregation of HA particles, which led to nozzle clogging and resulted in non-uniform printing (Figure 1b). The optimum scaffold chosen was P1H, which was referred to as PH in the subsequent surface modification studies.

The surface chemistry of the scaffolds was analyzed using FTIR, as depicted in Figure 2a. The P scaffold was utilized to detect peaks related to the PCL. The infrared spectrum exhibited peaks at 2949 cm^{-1} and 2864 cm^{-1}, corresponding to asymmetric and symmetric C-H stretches, respectively. The peaks detected at 1723, 1241, and 1188 cm^{-1} were assigned to the functional groups of carbonyl (C=O), ether (C-O & C-C), and cyclic ether (symmetric C-O-C), respectively [38]. The PP scaffold analysis revealed an increase in peak intensity at approximately 1723 cm^{-1} (C=O bond) when treating PCL with plasma. Furthermore, the spectral data exhibited two prominent peaks at 3443 and 1420 cm^{-1}, which were assigned to the stretching vibrations of O-H and C-O-C bonds, respectively. The presence of these peaks was due to the oxygen plasma treatment that introduces the carboxyl and hydroxyl functional groups onto the PCL surface via breaking the ester bonds of PCL in the polymer chain [39] (Figure 2b). In the spectrum of the PH scaffold, the appearance of two peaks at 3448-3572 cm^{-1} and 562-601 cm^{-1} can be attributed to OH and

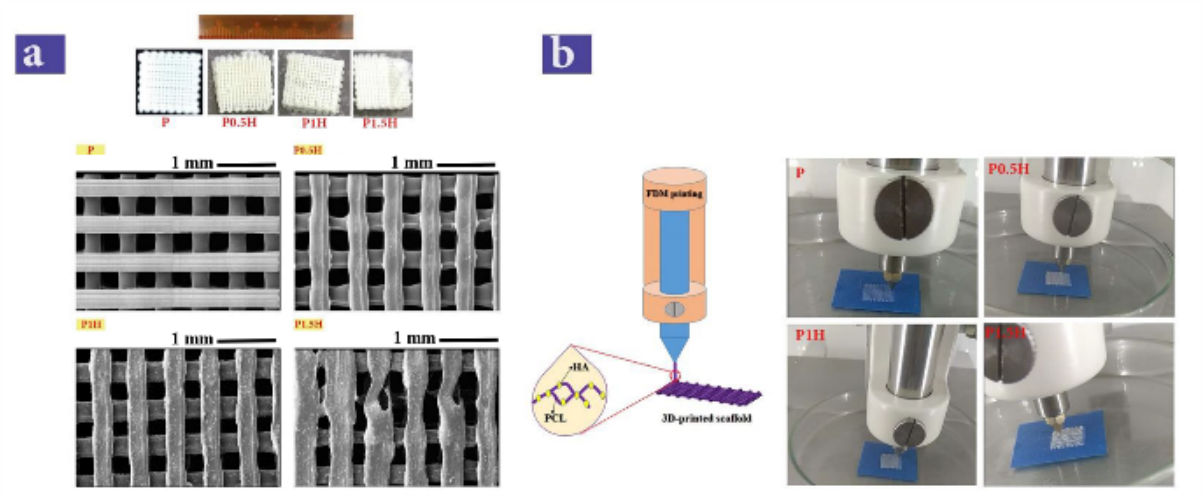

Figure 1. a) The created P, P0.5H, P1H, and P1.5H 3D printed scaffolds and their FESEM images, b) The 3D printing procedure used to fabricate the P, P0.5H, P1H, and P1.5H scaffolds

$(PO_4)_3$ groups in HA, respectively, which were not present in the P sample [40]. The chemical properties of PCL and simvastatin were found to be comparable. However, in the PHPS FTIR spectra, the vibrations of the OH group and peak displacements for C=O and ester were observed between 1724 and 1730 cm^{-1}, indicating the presence of the drug in the scaffold structure.

As seen in Figure 3, the addition of HA led to a decrease in the contact angle from 72.4 for pure PCL to 63.9 for the PH scaffold. Also, oxygen plasma led to a significant decrease in the contact angle to 40.7°. The PHPS scaffold exhibited a contact angle of 38.9.

The swelling capacity of the scaffolds was measured over 24 hours, and the results are demonstrated in Figure 4A. PCL showed only a 22.57±4.57% swelling ratio after 24 hours. In the HA-contained scaffolds, the swelling ratio was increased to 117.35±11.75% after 24 hours. The PHPS sample showed a higher swelling ratio at all measurement points [41], and final swelling ratio reaching 207.01±8.3%.

The biodegradability of scaffolds was measured by immersion in PBS solution, and the results are shown in Figure 4B. The percentage of biodegradation of scaffolds increased over time. Only 8.35±0.75% of P scaffolds were biodegraded within 21 days. After adding

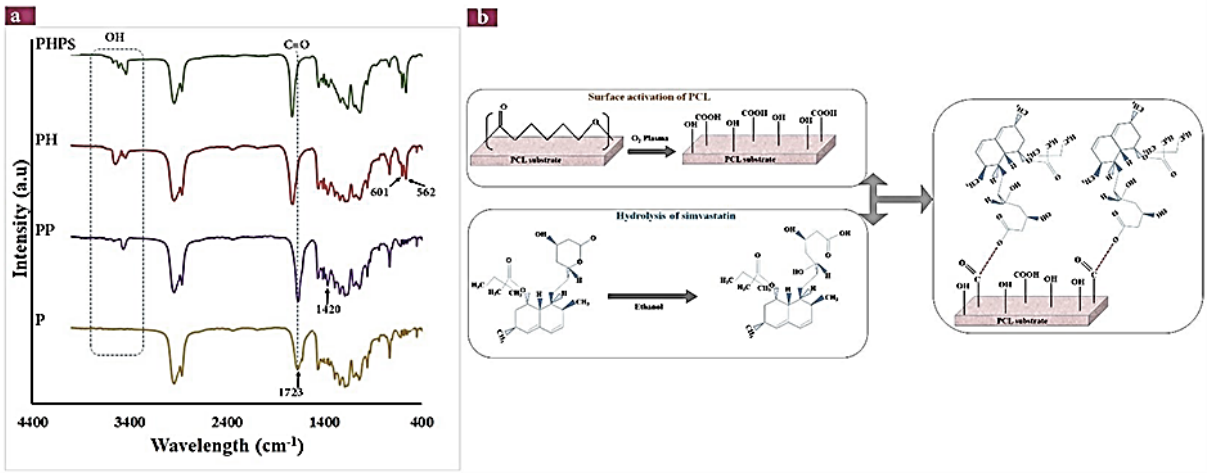

Figure 2. FTIR spectra of P, PP, PH, and PHPS samples (a) and the schematic of the proposed chemical reaction of the PHPS scaffold (b)

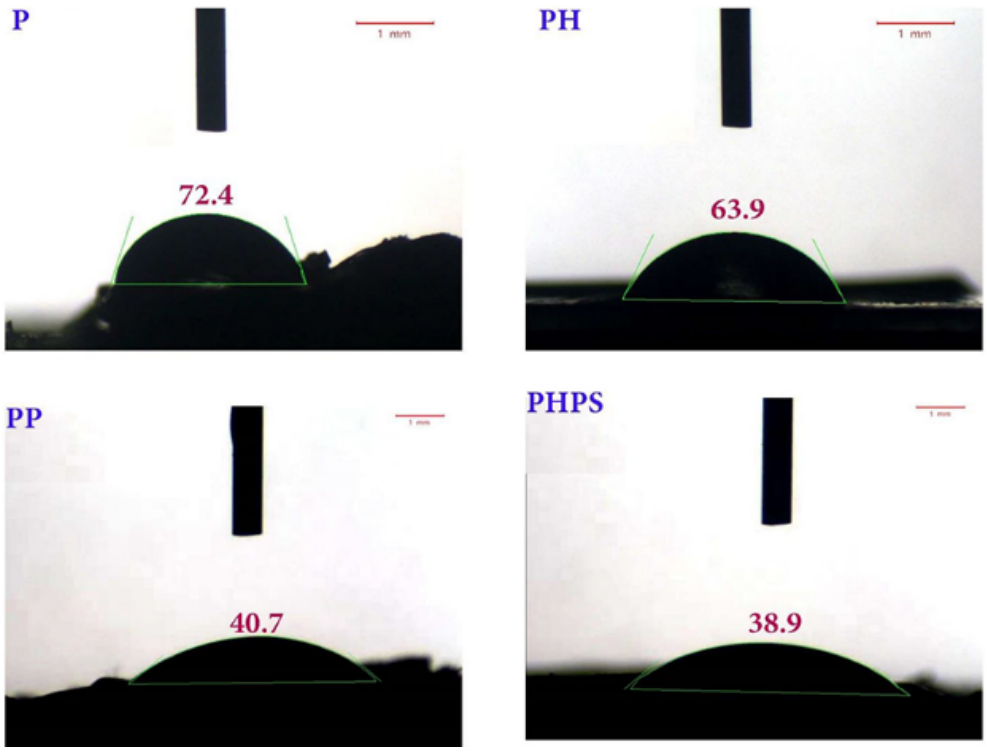

Figure 3. The contact angle measurement of P, PH, PP, and PHPS scaffolds

hydrophilic HA nanoparticles, the biodegradation rate reached 29.95±1.45% after 21 days. However, the PHPS sample showed the highest percentage of biodegradation among the samples, with its biodegradation ratio reaching 36.65±3.75% after 21 days.

The mechanical results (Figure 5) indicated that the P scaffold had a compressive strength of 5.27 MPa, which dramatically increased to 14.09 MPa in the PHPS scaffold.

Drug release results

The drug release results of the prepared scaffolds are shown in Figure 6. It can be seen that the drug release followed a linear model. According to the drug release kinetics, there was no drug release in the first hour in the PHS scaffold. After that, the drug release occurred very slowly over 7 hours, reaching a maximum drug release of 3%. In contrast, in the PHPS scaffold, the drug release rate initially increased linearly with time, and 90.99% of simvastatin was gradually released after 8 hours.

Biological properties of the 3D-printed scaffolds

On days 14 and 21, the ALP expression level of the cells grown on the constructed scaffolds was assessed (Figure 7A). The P scaffold showed no significant changes in ALP activity over time, whereas ALP activity significantly increased after 14 days in the PH and PHPS scaffolds. The ALP activity of the PH and PHPS scaffolds was considerably greater than that of the P scaffold after 14 and 21 days of incubation.

As shown in Figure 7B and C, calcium deposition on the PH and PHPS scaffolds was higher than that on the pure PCL scaffold, with the most significant calcium deposition observed in the PHPS group.

Figure 8 shows that the cells were alive and had almost similar cell morphological structures of F-actin on the PH and PHPS scaffolds after 21 days of culture. The results demonstrated that the proliferation and distribution of cells were more homogeneous in the PHPS scaffold compared to the PH scaffold.

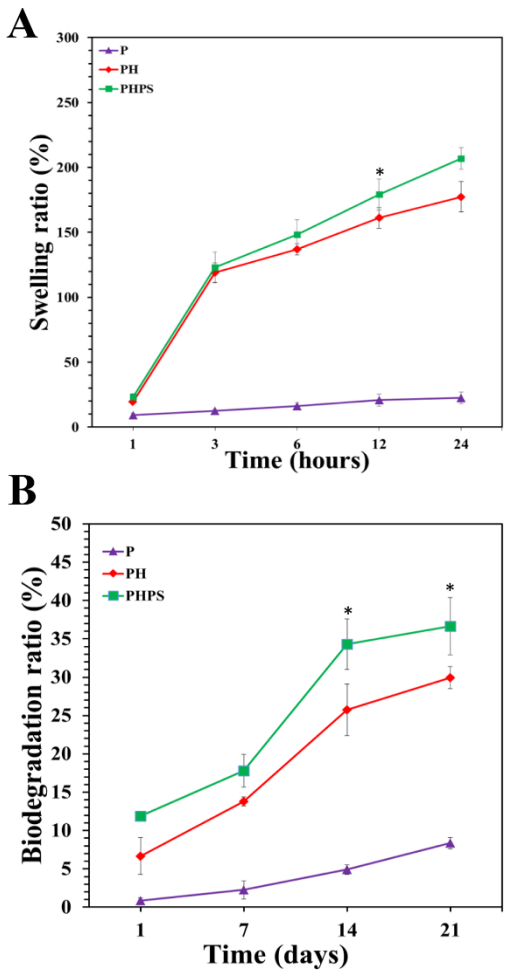

Figure 4. The swelling ratio (A) and biodegradation ratio (B) measurements of P, PH, PP, and PHPS scaffolds (*P<0.05)

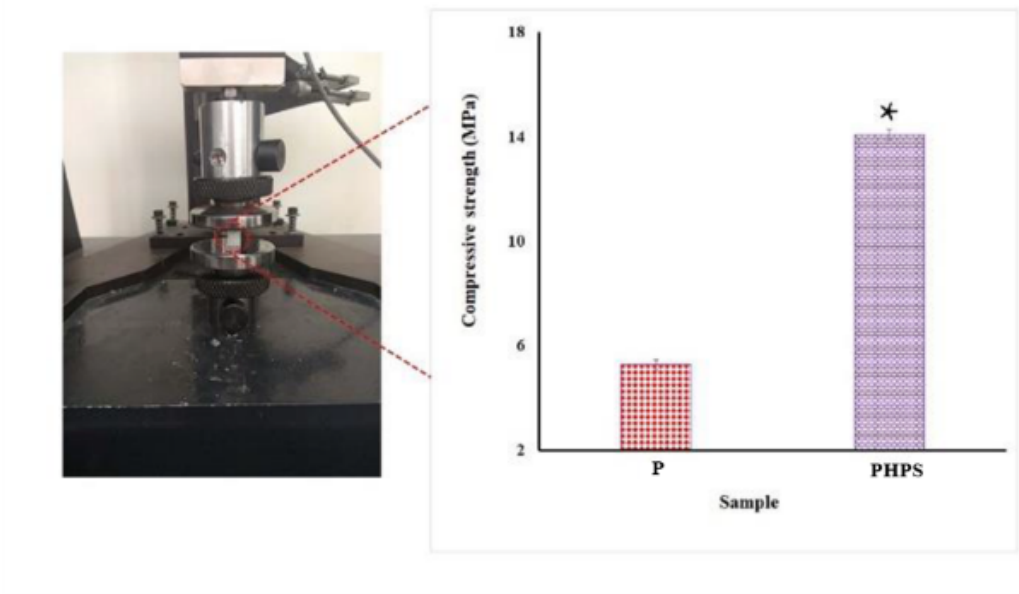

Figure 5. Mechanical investigation of P and PHPS scaffolds (*P<0.05)

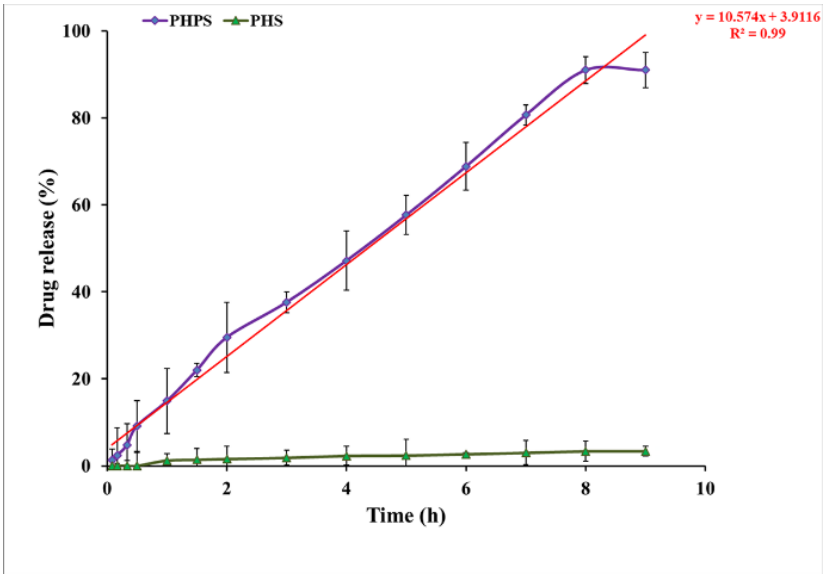

Figure 6. Simvastatin releases from the PHPS scaffold over 9 hours

Figure 9 shows the expression of BMP-2, OCN, and ALP in the P, PH, and PHPS scaffolds. After 14 days, the expression of BMP-2, OCN, and ALP increased, which indicated osteogenic differentiation of MC3T3 cells into mature osteoblasts. After 21 days, although the expression of BMP-2 and OCN increased, the ALP expression reduced.

Discussions

According to morphological observations, P1H was chosen as the optimum formulation for further studies due to its more uniform distribution of HA particles throughout the PCL scaffold compared to the other two samples. The interconnectivity of the scaffolds is an essential parameter for new bone regeneration because of the host cell migration from the native bone and the migration of the neighboring osteoblasts [42]. Furthermore, the percentage of porosity is an important factor in the design of tissue engineering scaffolds, as it provides sufficient space for cell migration, infiltration, vascularization, and material transportation [42, 43]. The P1H scaffold showed 70.3% porosity with interconnected pores, which is suitable for bone regeneration [44, 45].

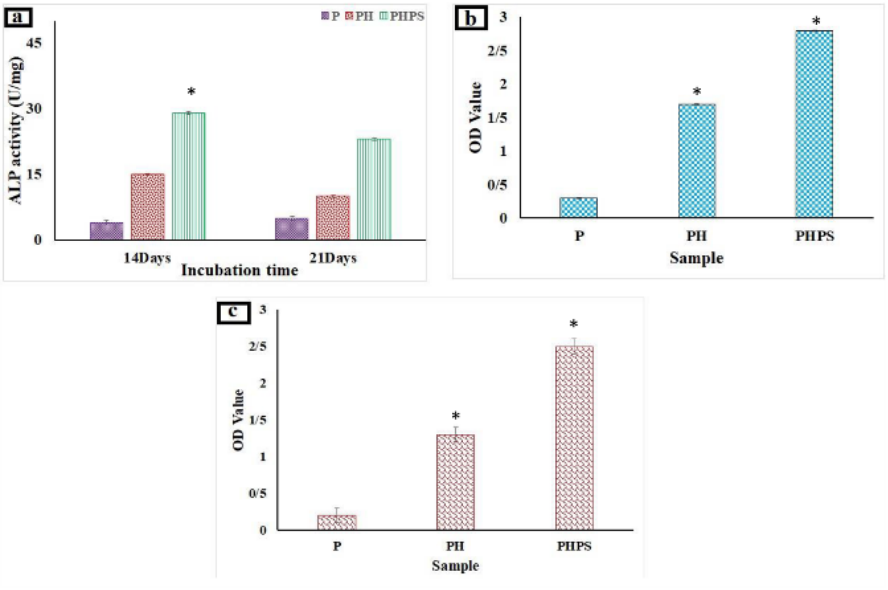

Figure 7. ALP activity (a), optical density (OD) values of ARS (b), and OCPC assay (c) of P, PH, and PHPS scaffolds (*P<0.05)

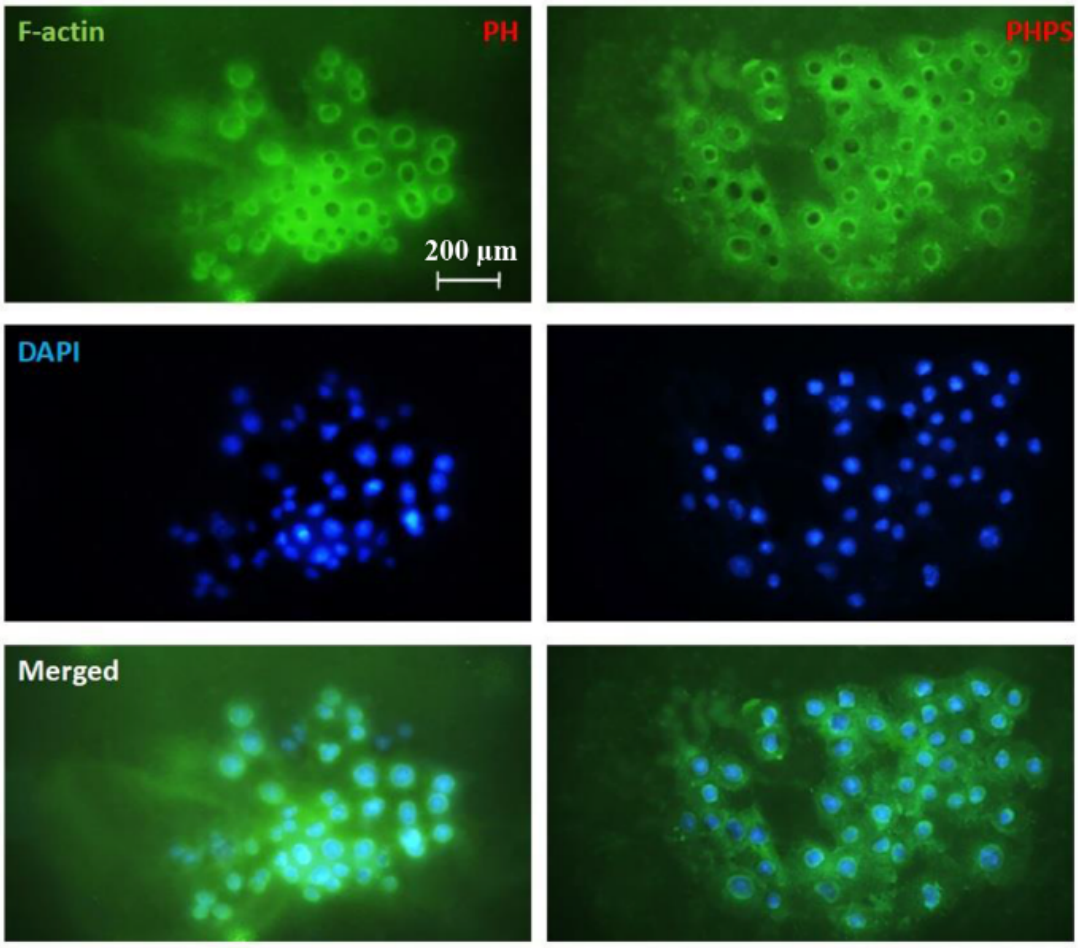

Figure 8. Fluorescence microscopy studies of F-actin organization (1st row), DAPI- labeled cell nuclei (2nd row), and the merged F-actin and DAPI (3rd row) of PH and PHPS scaffolds stained with phalloidin after 21 days

Note: DAPI staining of PH and PHPS scaffolds after 21 days.

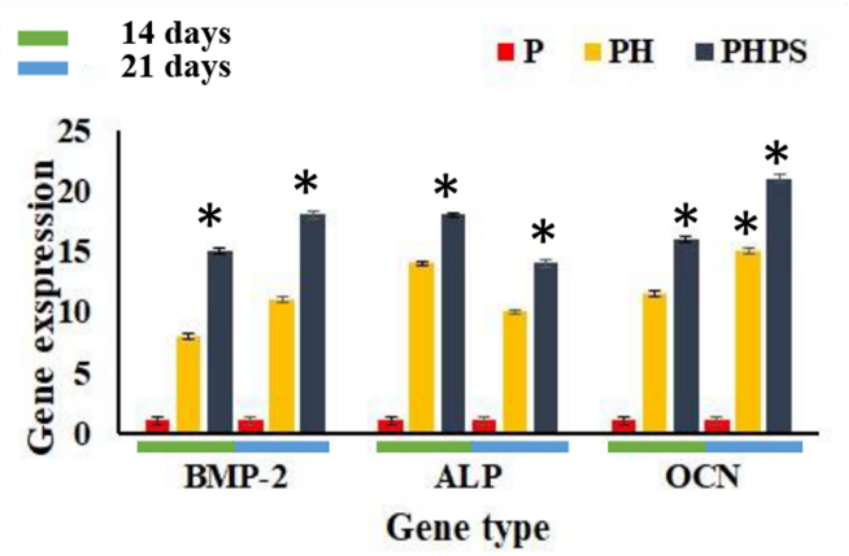

Figure 9. The expression of BMP-2, OCN, and ALP in the P, PH, and PHPS scaffolds (*P<0.05)

As PCL has a bioinert and hydrophobic nature, the plasma surface modification technique can modify the chemical and biological performances of PCL [46]. Plasma is being widely applied to improve the hydrophobicity of a material or to add predefined functional groups on the surface of a construct for further modification [47]. The plasma procedure offers several advantages, including the absence of solvents, resulting in reduced chemical reagent usage. Additionally, the highly energetic species generated by the procedure can create sterile conditions [48]. Oxygen plasma treatments produce surfaces that contain hydroxyl groups, allowing for the achievement of more stable coatings on the polymer surface. Simvastatin coating was performed on the PH scaffold after oxygen plasma modification, as confirmed by FTIR results.

The addition of HA led to a decrease in the contact angle, consistent with a previous study that attributed this to the hydrophilic nature of HA [49]. Furthermore, oxygen plasma treatment created active functional OH and COOH groups on the PH scaffold. The formation of hydrophilic bonds on the surface of PCL resulted in a higher interfacial adhesion tendency for molecular water, biopolymers, cells, or other biological components. These results indicate the successful incorporation of HA and simvastatin into PCL scaffolds.

Hydrophilicity affects the bio-performance of biomaterials, cell-biomaterial interactions, and the promotion of cellular adhesion and growth [50, 51]. The contact angle of the PHPS suggests that the combination of HA particles, plasma treatment, and simvastatin improved the hydrophilicity of PCL scaffolds. This improvement in the hydrophilicity of PCL was observed in a previous study by Ko et al. [52] after plasma treatment. The observed phenomenon may be attributed to the presence of hydrophilic moieties in both HA and plasma-treated surfaces.

Swelling ratio and biodegradability are also important parameters in the design of bone tissue engineering scaffolds. Scaffolds act as a temporary biomimetic framework of the ECM, which is replaced by cell growth and tissue repair [53].

The results of the swelling tests were consistent with the hydrophilicity evaluations. According to the results, all samples showed increased water absorption within 24 hours. PCL did not exhibit much affinity for water molecules due to its relatively hydrophobic nature within this time frame [54]. However, HA-containing scaffolds presented a higher swelling ratio due to increased hydrophilicity. Surface modification with plasma created hydrophilic functional groups on the surface of the scaffold, and facilitated the interaction with water molecules, thereby increasing the swelling ratio.

PCL had a low biodegradation ratio due to its hydrophobic nature and its high crystallinity [55]. After adding hydrophilic HA nanoparticles, the biodegradation rate of scaffolds increased. PCL biodegradation occurred in two amorphous and crystalline phases. Firstly, the amorphous phase and then the crystalline phase were degraded. The incorporation of additives, such as HA accelerates PCL biodegradation from weeks to even days. The higher slope observed between 7 and 14 days in the PH and PHPS samples can be attributed to this acceleration of PCL biodegradation following the addition of HA [56]. The increased biodegradation in PHPS was due to the addition of hydrophilic HA nanoparticles and surface modification with hydrophilic groups. According to the results of hydrophilicity and swelling ratio, the biodegradation results were as expected. The results of the swelling and biodegradation tests were consistent with a previous study on PCL/bioactive glass scaffolds, which found that plasma treatments and simvastatin loading enhanced the swelling capacity and accelerated the biodegradation rate [32].

The mechanical stability of scaffolds is also an essential factor for bone tissue regeneration [57]. This importance arises because growing cells may apply force, and shape changes in a mechanically weak scaffold can affect the final tissue structure [58]. Mechanical tests were performed on the P and PHPS scaffolds. The composite PCL, with a bone-mimetic structure and a uniform distribution of bioceramic particles in the PCL polymer matrix, was chosen as a strategy to increase the mechanical properties of PCL-based scaffolds [59]. The increase in the mechanical properties of PHPS can be primarily attributed to the introduced HA nanoparticles [60]. Therefore, the results exhibited that the presence of HA in the PCL matrix improved the mechanical properties of the scaffold by approximately 2.67 times. This behavior may indicate that evenly distributed HA particles within the PCL matrix developed friction, enabling the PCL to sustain the load.

The drug release profiles of the samples were modeled by the zero-order equation (Equation 3):

3. $Q_t = Q_0 + kt$

Qt is the cumulative amount of drug released at a time "t"; Q_0 is the initial amount of drug; k and t are the zero-order constant and time in hours, respectively.

PCL is intrinsically a hydrophobic polymer, and the small amount of adsorbed simvastatin was due to the presence of HA in the PCL matrix. The interaction between the OH groups in the HA structure and the COOH groups in the hydrolyzed simvastatin structure facilitated the adsorption of simvastatin onto the PHPS scaffold. Plasma treatment of the PH surface formed OH and COOH functional groups, which led to high adsorption of simvastatin on the surface through interactions between simvastatin molecules and the functional groups as active sites on the PHPS surface.

Selecting the appropriate biomaterial for tissue engineering scaffold fabrication, along with obtaining high cell adhesion, is a significant concern in this context [61]. ALP is an early marker of immature osteoblast activity and plays a vital role in forming bone minerals [62]. Both the production of extracellular matrix (ECM) and osteogenic differentiation depend on an increase in ALP activity. The combination of HA and simvastatin contributes to this increase, indicating osteoblast maturation. HA is the main inorganic ingredient of bone tissue, and its high cell interactions are related to its bioactivity, osteoconductivity, and hydrophilicity [63]. The higher cellular interaction observed in the PHPS sample can be attributed to its greater hydrophilicity and swelling ratio. However, there was a decrease in ALP activity at day 21, indicating that the pre-osteoblast MC3T3 cells had differentiated [64]. This level of ALP activity was 3.8 (PH) and 7.2 (PHPS) times higher than that of ALP in pure PCL (P) after 21 days.

Calcium is a crucial mineral that is indispensable for the survival of all living organisms. Its ability to sequester and release Ca^{2+} serves as a signal for numerous cellular processes. The differentiated osteoblasts from MC3T3s can deposit calcium in the ECM during the mineralization procedure [65]. Therefore, ARS staining and OCPC assay were performed to indicate successful ECM mineralization and to measure calcium deposition in the ECM on the scaffolds after 21 days. The results of calcium deposition suggest that the combination of HA and simvastatin had a greater impact on mineralization compared to the PCL scaffold alone. Additionally, the study found evidence of a synergistic effect between HA and simvastatin in promoting calcium deposition. The simvastatin-coated PH composite was found to enhance cell proliferation and osteogenic behavior, as confirmed by both ARS and OCPC.

The PHPS scaffolds exhibited improved cell adherence due to the addition of HA to the PCL scaffold and the consistent application of simvastatin coating. Consequently, the qualitative outcomes proved that cell growth, proliferation, and differentiation could all be supported by the PHPS scaffold within the scaffolds. Hydrophilic environments are a crucial factor in scaffold surface design within the field of tissue engineering. The modification of hydrophobic scaffolds has the potential to alter their surface properties, leading to enhanced cellular attachment, growth, and proliferation [66]. This hydrophilic environment and osteogenic substrate were provided by the incorporation of HA and simvastatin into the PCL scaffold.

The reduction in ALP expression after 21 days in the scaffolds may signify the terminal differentiation of osteoblast cells and their transformation from the differentiation phase to the proliferation phase. BMP-2 is a secretory signaling molecule that plays an essential role in the induction of osteoblast differentiation by influencing different osteoblast differentiation processes at different stages [67, 68]. Simvastatin could promote osteogenesis by activating osteogenesis-related signal transduction pathways. Furthermore, simvastatin enhanced osteoblast viability and differentiation by activating the Ras/Smad/Erk/BMP-2 signaling pathway [28]. The effective mechanism of simvastatin in bone regeneration is related to enhanced BMP-2 expression and inhibited osteoclasts by blocking the prenylation of small guanosine triphosphatase (GTPase) proteins.

GTPase proteins exist in an inactive state, where they are bound to guanosine diphosphate (GDP) within the cytoplasm. During the cell activation phase, GTP is exchanged and transferred to a membrane form that is active. In contrast, it is imperative for small GTPase proteins to undergo prenylation in order to effectively attach to cellular membranes. The prenylated small GTPase proteins play a crucial role in activating osteoclasts and inhibiting BMP-2 synthesis and osteoblasts, by acting on downstream signaling pathways [61, 62]. Furthermore, the ALP enzyme is responsible for the provision of inorganic phosphate, which is essential for the mineralization process. The non-collagenous protein, OCN, is highly prevalent in bone tissue, particularly in osteoblast lineage cells, such as mature osteoblasts [63]. PHPS had a significant impact on the transcription of ALP, OCN, and BMP-2 in MC3T3-E1 pre-osteoblasts. Moreover, it has been suggested that the administration of simvastatin may lead to an upregulation of the BMP-2 signaling pathway, which in turn could result in elevated levels of ALP and OCN activity. The findings of this study sug-

gest that the addition of HA and simvastatin coating to the PCL scaffold can improve cellular responses, leading to increased cell proliferation and differentiation. HA presented a mimicked bioactive microenvironment of the native inorganic phase of bone tissue. On the other hand, simvastatin could accelerate mineral deposition.

Conclusion

3D-printed composite PCL/HA/simvastatin (PHPS) scaffolds were fabricated using fused deposition modeling 3D Printing. Results indicated that scaffolds loaded with HA and simvastatin enhanced cell adhesion, proliferation, and differentiation. Simvastatin-loaded scaffolds exhibited significant levels of biological activity and promoted biomineralization. The surface modification and the addition of HA to the PCL scaffold enhanced the hydrophilicity of the scaffolds, resulting in greater swelling and biodegradation ratios. Simvastatin and HA both had beneficial effects on cell adhesion and proliferation compared to pure PCL in vitro, which can be attributed to their complementary actions, as well as the existence of a 3D structure with interconnected porosity. Therefore, applications for bone tissue engineering may be possible for 3D-printed PHPS scaffolds.

Ethical Considerations

Compliance with ethical guidelines

There were no ethical considerations to be considered in this research.

Funding

This research did not receive any grant from funding agencies in the public, commercial, or non-profit sectors.

Authors' contributions

All authors contributed equally to the conception and design of the study, data collection and analysis, interception of the results and drafting of the manuscript. Each author approved the final version of the manuscript for submission.

Conflict of interest

The authors declared no conflict of interest.

References

[1] Norouzi M, Naderi MN, Komasi MH, Sharifzadeh SR, Shahrezaei M, Eajazi A. Clinical results of using the proximal humeral internal locking system plate for internal fixation of displaced proximal humeral fractures. The American Journal of Orthopedics. 2012; 41(5):E64-8. [Link]

[2] Haghighizadeh E, Shahrezaee M, Sharifzadeh S, Momeni M. Transforming growth factor-β3 relation with osteoporosis and osteoporotic fractures. Journal of Research in Medical Sciences. 2019; 24(1):46. [DOI:10.4103/jrms.JRMS_1062_18] [PMID]

[3] Hassanzadeh Nemati N, Mirhadi SM. Synthesis and characterization of highly porous TiO2 scaffolds for bone defects. International Journal of Engineering. 2020; 33(1):134-40. [DOI:10.5829/ije.2020.33.01a.15]

[4] Liu D, Nie W, Li D, Wang W, Zheng L, Zhang J, et al. 3D printed PCL/SrHA scaffold for enhanced bone regeneration. Chemical Engineering Journal. 2019; 362:269-79. [DOI:10.1016/j.cej.2019.01.015]

[5] Rezaei H, Shahrezaee M, Monfared MJ, Nikjou M, Shahrezaee MH, Mohseni M. Fabrication and characterization of three-dimensional polycaprolactone/sodium alginate and egg whites and eggshells hybrid scaffold in bone tissue engineering. Journal of Polymer Engineering. 2023; 43(1):47-52. [DOI:10.1515/polyeng-2022-0138]

[6] Sultana N, Hassan MI, Ridzuan N, Ibrahim Z, Soon CF. Fabrication of gelatin scaffolds using thermally induced phase separation technique. International Journal of Engineering. 2018; 31(8):1302-7. [DOI:10.5829/ije.2018.31.08b.19]

[7] Wang W, Huang B, Byun JJ, Bártolo P. Assessment of PCL/carbon material scaffolds for bone regeneration. Journal of the Mechanical Behavior of Biomedical Materials. 2019; 93:52-60. [DOI:10.1016/j.jmbbm.2019.01.020] [PMID]

[8] Karageorgiou V, Kaplan D. Porosity of 3D biomaterial scaffolds and osteogenesis. Biomaterials. 2005; 26(27):5474-91. [DOI:10.1016/j.biomaterials.2005.02.002] [PMID]

[9] Hannink G, Arts JJ. Bioresorbability, porosity and mechanical strength of bone substitutes: What is optimal for bone regeneration? Injury. 2011; 42(Suppl 2):S22-5. [DOI:10.1016/j.injury.2011.06.008] [PMID]

[10] Sarparast Z, Abdoli R, Rahbari A, Varmazyar M, Kashyzadeh KR. Experimental and Numerical Analysis of Permeability in Porous Media. International Journal of Engineering. 2020; 33(11):2408-15. [DOI:10.5829/ije.2020.33.11b.31]

[11] Ghorbani F, Zamanian A, Sahranavard M. Mussel-inspired polydopamine-mediated surface modification of freeze-cast poly (ε-caprolactone) scaffolds for bone tissue engineering applications. Biomedical Engineering. 2020; 65(3):273-87. [DOI:10.1515/bmt-2019-0061] [PMID]

[12] Park JY, Jang J, Kang HW. 3D Bioprinting and its application to organ-on-a-chip. Microelectronic Engineering. 2018; 200:1-11. [DOI:10.1016/j.mee.2018.08.004]

[13] Hutmacher DW, Schantz T, Zein I, Ng KW, Teoh SH, Tan KC. Mechanical properties and cell cultural response of polycaprolactone scaffolds designed and fabricated via fused deposition modeling. Journal of Biomedical Materials Research. 2001; 55(2):203-16. [DOI:10.1002/1097-4636(200105)55:23.3.CO;2-Z] [PMID]

[14] Sahranavard M, Zamanian A, Ghorbani F, Shahrezaee MH. A critical review on three dimensional-printed chitosan hydrogels for development of tissue engineering. Bioprinting. 2019; 17:e00063. [DOI:10.1016/j.bprint.2019.e00063]

[15] Sahranavard M, Sarkari S, Safavi S, Ghorbani F. Three-dimensional bio-printing of decellularized extracellular matrix-based bio-inks for cartilage regeneration: A systematic review. Biomaterials Translational. 2022; 3(2):105-15. [DOI:10.12336/biomatertransl.2022.02.004] [PMID]

[16] Ghaee A, Bagheri-Khoulenjani S, Amir Afshar H, Bogheiri H. Biomimetic nanocomposite scaffolds based on surface modified PCL-nanofibers containing curcumin embedded in chitosan/gelatin for skin regeneration. Composites Part B: Engineering. 2019; 177:107339. [DOI:10.1016/j.compositesb.2019.107339]

[17] Yang X, Wang Y, Zhou Y, Chen J, Wan Q. The application of polycaprolactone in three-dimensional printing scaffolds for bone tissue engineering. Polymers. 2021; 13(16):2754. [DOI:10.3390/polym13162754] [PMID]

[18] Sruthi R, Balagangadharan K, Selvamurugan N. Polycaprolactone/polyvinylpyrrolidone coaxial electrospun fibers containing veratric acid-loaded chitosan nanoparticles for bone regeneration. Colloids and Surfaces. B, Biointerfaces. 2020; 193:111110. [DOI:10.1016/j.colsurfb.2020.111110] [PMID]

[19] Park SA, Lee HJ, Kim SY, Kim KS, Jo DW, Park SY. Three-dimensionally printed polycaprolactone/beta-tricalcium phosphate scaffold was more effective as an rhBMP-2 carrier for new bone formation than polycaprolactone alone. Journal of Biomedical Materials Research. Part A. 2021; 109(6):840-8. [DOI:10.1002/jbm.a.37075] [PMID]

[20] Duymaz BT, Erdiler FB, Alan T, Aydogdu MO, Inan AT, Ekren N, et al. 3D bio-printing of levan/polycaprolactone/gelatin blends for bone tissue engineering: Characterization of the cellular behavior. European Polymer Journal. 2019; 119:426-37. [DOI:10.1016/j.eurpolymj.2019.08.015]

[21] Juan PK, Fan FY, Lin WC, Liao PB, Huang CF, Shen YK, et al. Bioactivity and bone cell formation with poly-ε-caprolactone/bioceramic 3d porous scaffolds. Polymers. 2021; 13(16):2718. [DOI:10.3390/polym13162718] [PMID]

[22] Park SA, Lee SJ, Seok JM, Lee JH, Kim WD, Kwon IK. Fabrication of 3D printed PCL/PEG polyblend scaffold using rapid prototyping system for bone tissue engineering application. Journal of Bionic Engineering. 2018; 15(3):435-42. [DOI:10.1007/s42235-018-0034-8]

[23] Arabahmadi S, Pezeshki Modaress M, Irani S, Zandi M. Electrospun biocompatible gelatin-chitosan/polycaprolactone/hydroxyapatite nanocomposite scaffold for bone tissue engineering. International Journal of Nano Dimension. 2018; 10(2):169-79. [Link]

[24] Pitjamit S, Thunsiri K, Nakkiew W, Wongwichai T, Pothacharoen P, Wattanutchariya W. The possibility of interlocking nail fabrication from FFF 3D printing PLA/PCL/HA composites coated by local silk fibroin for canine bone fracture treatment. Materials. 2020; 13(7):1564. [DOI:10.3390/ma13071564] [PMID]

[25] Mirică IC, Furtos G, Lucaciu O, Pascuta P, Vlassa M, Moldovan M, et al. Electrospun membranes based on polycaprolactone, nano-hydroxyapatite and metronidazole. Materials. 2021; 14(4):931. [DOI:10.3390/ma14040931] [PMID]

[26] Roh HS, Lee CM, Hwang YH, Kook MS, Yang SW, Lee D, et al. Addition of MgO nanoparticles and plasma surface treatment of three-dimensional printed polycaprolactone/hydroxyapatite scaffolds for improving bone regeneration. Materials Science & Engineering. C, Materials for Biological Applications. 2017; 74:525-35. [DOI:10.1016/j.msec.2016.12.054] [PMID]

[27] Shahrezaee M, Oryan A, Bastami F, Hosseinpour S, Shahrezaee MH, Kamali A. Comparative impact of systemic delivery of atorvastatin, simvastatin, and lovastatin on bone mineral density of the ovariectomized rats. Endocrine. 2018; 60(1):138-50. [DOI:10.1007/s12020-018-1531-6] [PMID]

[28] Chen PY, Sun JS, Tsuang YH, Chen MH, Weng PW, Lin FH. Simvastatin promotes osteoblast viability and differentiation via Ras/Smad/Erk/BMP-2 signaling pathway. Nutrition Research. 2010; 30(3):191-9. [DOI:10.1016/j.nutres.2010.03.004] [PMID]

[29] Feng C, Xiao L, Yu JC, Li DY, Tang TY, Liao W, et al. Simvastatin promotes osteogenic differentiation of mesenchymal stem cells in rat model of osteoporosis through BMP-2/Smads signaling pathway. European Review for Medical & Pharmacological Sciences. 2020; 24(1):434-43. [Link]

[30] Rezaei H, Shahrezaee M, Jalali Monfared M, Fathi Karkan S, Ghafelehbashi R. Simvastatin-loaded graphene oxide embedded in polycaprolactone-polyurethane nanofibers for bone tissue engineering applications. Journal of Polymer Engineering. 2021; 41(5):375-86. [DOI:10.1515/polyeng-2020-0301]

[31] Jacobs T, Morent R, De Geyter N, Dubruel P, Leys C. Plasma surface modification of biomedical polymers: Influence on cell-material interaction. Plasma Chemistry and Plasma Processing. 2012; 32(5):1039-73. [DOI:10.1007/s11090-012-9394-8]

[32] Ghorbani F, Ghalandari B, Sahranavard M, Zamanian A, Collins MN. Tuning the biomimetic behavior of hybrid scaffolds for bone tissue engineering through surface modifications and drug immobilization. Materials Science & Engineering. C, Materials for Biological Applications. 2021; 130:112434. [DOI:10.1016/j.msec.2021.112434] [PMID]

[33] Wang F, Tankus EB, Santarella F, Rohr N, Sharma N, Märtin S, et al. Fabrication and characterization of PCL/HA filament as a 3D printing material using thermal extrusion technology for bone tissue engineering. Polymers. 2022; 14(4):669. [DOI:10.3390/polym14040669] [PMID]

[34] Visscher DO, Lee H, van Zuijlen PPM, Helder MN, Atala A, Yoo JJ, et al. A photo-crosslinkable cartilage-derived extracellular matrix bioink for auricular cartilage tissue engineering. Acta Biomaterialia. 2021; 121(1):193-203. [DOI:10.1016/j.actbio.2020.11.029] [PMID]

[35] Ghorbani F, Pourhaghgouy M, Mohammadi-hafshehjani T, Zamanian A. Effect of silane-coupling modification on the performance of chitosan-poly vinyl alcohol-hybrid scaffolds in bone tissue engineering. Silicon. 2020; 12: 3015–26. [DOI:10.1007/s12633-020-00397-2]

[36] Cyster LA, Grant DM, Howdle SM, Rose FRAJ, Irvine DJ, Freeman D, et al. The influence of dispersant concentration on the pore morphology of hydroxyapatite ceramics for bone tissue engineering. Biomaterials. 2005; 26(7):697-702. [DOI:10.1016/j.biomaterials.2004.03.017] [PMID]

[37] Zaharin H, Abdul Rani A, Azam F, Ginta T, Sallih N, Ahmad A, et al. Effect of unit cell type and pore size on porosity and mechanical behavior of additively manufactured Ti6Al4V scaffolds. Materials. 2018; 11(12):2402. [DOI:10.3390/ma11122402] [PMID]

[38] Jafari A, Amirsadeghi A, Hassanajili S, Azarpira N. Bioactive antibacterial bilayer PCL/gelatin nanofibrous scaffold promotes full-thickness wound healing. International Journal of Pharmaceutics. 2020; 583:119413. [DOI:10.1016/j.ijpharm.2020.119413] [PMID]

[39] Martins A, Pinho ED, Faria S, Pashkuleva I, Marques AP, Reis RL, et al. Surface modification of electrospun polycaprolactone nanofiber meshes by plasma treatment to enhance biological performance. Small. 2009; 5(10):1195-206. [DOI:10.1002/smll.200801648] [PMID]

[40] Maji K, Dasgupta S. Characterization and in vitro evaluation of gelatin-chitosan scaffold reinforced with bioceramic nanoparticles for bone tissue engineering. Journal of Materials Research. 2019; 34(16):2807-18. [DOI:10.1557/jmr.2019.170]

[41] Choi YM, Im SJ, Myung SW, Choi HS, Park KN, Huh KM. Preparation and swelling behavior of superporous hydrogels: Control of pore structure and surface property. Key Engineering Materials. 2007; 342-343:717-20. [DOI:10.4028/www.scientific.net/KEM.342-343.717]

[42] Abbasi N, Hamlet S, Love RM, Nguyen NT. Porous scaffolds for bone regeneration. Journal of Science: Advanced Materials and Devices. 2020; 5(1):1-9. [DOI:10.1016/j.jsamd.2020.01.007]

[43] Cheng M qi, Wahafu T, Jiang G feng, Liu W, Qiao Y qin, Peng X chun, et al. A novel open-porous magnesium scaffold with controllable microstructures and properties for bone regeneration. Scientific Reports. 2016; 6(1):24134. [DOI:10.1038/srep24134] [PMID]

[44] Dziaduszewska M, Zieliński A. Structural and material determinants influencing the behavior of porous Ti and its alloys made by additive manufacturing techniques for biomedical applications. Materials. 2021; 14(4):712. [DOI:10.3390/ma14040712] [PMID]

[45] Wang X, Zhu Z, Xiao H, Luo C, Luo X, Lv F, et al. Three-dimensional, multiscale, and interconnected trabecular bone mimic porous tantalum scaffold for bone tissue engineering. ACS Omega. 2020; 5(35):22520-8. [DOI:10.1021/acsomega.0c03127] [PMID]

[46] Siri S, Wadbua P, Amornkitbamrung V, Kampa N, Maensiri S. Surface modification of electrospun PCL scaffolds by plasma treatment and addition of adhesive protein to promote fibroblast cell adhesion. Materials Science and Technology. 2010; 26(11):1292-7. [DOI:10.1179/026708310X12798718274070]

[47] Chu P. Plasma-surface modification of biomaterials. Materials Science and Engineering: R: Reports. 2002; 36(5-6):143-206. [DOI:10.1016/S0927-796X(02)00004-9]

[48] Domingos M, Intranuovo F, Gloria A, Gristina R, Ambrosio L, Bártolo PJ, et al. Improved osteoblast cell affinity on plasma-modified 3-D extruded PCL scaffolds. Acta Biomaterialia. 2013; 9(4):5997-6005. [DOI:10.1016/j.actbio.2012.12.031] [PMID]

[49] Hassan MI, Sultana N, Hamdan S. Bioactivity assessment of poly (caprolactone)/hydroxyapatite electrospun fibers for bone tissue engineering application. Journal of Nanomaterials. 2014; 2014(1):573238. [DOI:10.1155/2014/573238]

[50] Paterlini TT, Nogueira LFB, Tovani CB, Cruz MAE, Derradi R, Ramos AP. The role played by modified bioinspired surfaces in interfacial properties of biomaterials. Biophysical Reviews. 2017; 9(5):683-98. [DOI:10.1007/s12551-017-0306-2] [PMID]

[51] Gaharwar AK, Singh I, Khademhosseini A. Engineered biomaterials for in situ tissue regeneration. Nature Reviews Materials. 2020; 5(9):686-705. [DOI:10.1038/s41578-020-0209-x]

[52] Ko YM, Choi DY, Jung SC, Kim BH. Characteristics of plasma treated electrospun polycaprolactone (PCL) nanofiber scaffold for bone tissue engineering. Journal of Nanoscience and Nanotechnology. 2015; 15(1):192-5. [DOI:10.1166/jnn.2015.8372] [PMID]

[53] Guarino V, Raucci MG, Ronca A, Cirillo V, Ambrosio L. Multifunctional scaffolds for bone regeneration. In: Mallick K, editor. Bone substitute biomaterials. Sawston: Woodhead Publishing; 2014. [DOI:10.1533/9780857099037.2.95]

[54] Shie Karizmeh M, Poursamar SA, Kefayat A, Farahbakhsh Z, Rafienia M. An in vitro and in vivo study of PCL/chitosan electrospun mat on polyurethane/propolis foam as a bilayer wound dressing. Materials Science & Engineering. C, Materials for Biological Applications. 2022; 135:112667. [DOI:10.1016/j.msec.2022.112667] [PMID]

[55] Dethe MR, A P, Ahmed H, Agrawal M, Roy U, Alexander A. PCL-PEG copolymer based injectable thermosensitive hydrogels. Journal of Controlled Release. 2022; 343:217-36. [DOI:10.1016/j.jconrel.2022.01.035] [PMID]

[56] Doyle SE, Henry L, Mcgennisken E. Characterization of polycaprolactone nanohydroxyapatite composites with tunable degradability suitable for indirect printing. Polymers. 2021; 13(2):295. [DOI:10.3390/polym13020295] [PMID]

[57] Bahrami S, Baheiraei N, Shahrezaee M. Biomimetic reduced graphene oxide coated collagen scaffold for in situ bone regeneration. Scientific Reports. 2021; 11(1):16783. [DOI:10.1038/s41598-021-96271-1] [PMID]

[58] Gregor A, Filová E, Novák M, Kronek J, Chlup H, Buzgo M, et al. Designing of PLA scaffolds for bone tissue replacement fabricated by ordinary commercial 3D printer. Journal of Biological Engineering. 2017; 11(1):31. [DOI:10.1186/s13036-017-0074-3] [PMID]

[59] Wei G, Ma PX. Structure and properties of nano-hydroxyapatite/polymer composite scaffolds for bone tissue engineering. Biomaterials. 2004; 25(19):4749-57. [DOI:10.1016/j.biomaterials.2003.12.005] [PMID]

[60] Verma N, Zafar S, Talha M. Influence of nano-hydroxyapatite on mechanical behavior of microwave processed polycaprolactone composite foams. Materials Research Express. 2019; 6(8):085336. [DOI:10.1088/2053-1591/ab260d]

[61] Schlie-Wolter S, Ngezahayo A, Chichkov BN. The selective role of ECM components on cell adhesion, morphology, proliferation and communication in vitro. Experimental Cell Research. 2013; 319(10):1553-61. [DOI:10.1016/j.yexcr.2013.03.016] [PMID]

[62] Golub EE, Boesze-Battaglia K. The role of alkaline phosphatase in mineralization. Current Opinion in Orthopaedics. 2007; 18(5):444-8. [DOI:10.1097/BCO.0b013e3282630851]

[63] Domingos M, Gloria A, Coelho J, Bartolo P, Ciurana J. Three-dimensional printed bone scaffolds: The role of nano/micro-hydroxyapatite particles on the adhesion and differentiation of human mesenchymal stem cells. Proceedings of the Institution of Mechanical Engineers. Part H, Journal of Engineering in Medicine. 2017; 231(6):555-64. [DOI:10.1177/0954411916680236] [PMID]

[64] Kuo ZK, Lai PL, Toh EKW, Weng CH, Tseng HW, Chang PZ, et al. Osteogenic differentiation of preosteoblasts on a hemostatic gelatin sponge. Scientific Reports. 2016; 6(1):32884. [DOI:10.1038/srep32884] [PMID]

[65] Addison WN, Nelea V, Chicatun F, Chien YC, Tran-Khanh N, Buschmann MD, et al. Extracellular matrix mineralization in murine MC3T3-E1 osteoblast cultures: An ultrastructural, compositional and comparative analysis with mouse bone. Bone. 2015; 71:244-56. [DOI:10.1016/j.bone.2014.11.003] [PMID]

[66] Ferrari M, Cirisano F, Morán MC. Mammalian cell behavior on hydrophobic substrates: Influence of surface properties. Colloids and Interfaces. 2019; 3(2):48. [DOI:10.3390/colloids3020048]

[67] Xu Y, Yang Y, Hua Z, Li S, Yang Z, Liu Q, et al. BMP2 immune complexes promote new bone formation by facilitating the direct contact between osteoclasts and osteoblasts. Biomaterials. 2021; 275:120890. [DOI:10.1016/j.biomaterials.2021.120890] [PMID]

[68] Huntley R, Jensen E, Gopalakrishnan R, Mansky KC. Bone morphogenetic proteins: Their role in regulating osteoclast differentiation. Bone Reports. 2019; 10:100207. [DOI:10.1016/j.bonr.2019.100207] [PMID]